Nanogap-Enhanced Infrared Spectroscopy with Template-Stripped Wafer-Scale Arrays of Buried Plasmonic Cavities

ARTICLE *in* NANO LETTERS · NOVEMBER 2014

Impact Factor: 13.59 · DOI: 10.1021/nl503126s · Source: PubMed

4 AUTHORS, INCLUDING:

Xiaoshu Chen
University of Minnesota Twin Cities
18 PUBLICATIONS **107** CITATIONS
SEE PROFILE

Cristian Ciracì
Istituto Italiano di Tecnologia
36 PUBLICATIONS **586** CITATIONS
SEE PROFILE

NANO LETTERS

Letter

pubs.acs.org/NanoLett

Nanogap-Enhanced Infrared Spectroscopy with Template-Stripped Wafer-Scale Arrays of Buried Plasmonic Cavities

Xiaoshu Chen,[†] Cristian Ciracì,[‡,§] David R. Smith,[§] and Sang-Hyun Oh*[,†]

[†]Department of Electrical and Computer Engineering, University of Minnesota, Minneapolis, Minnesota 55455, United States

[‡]Center for Biomolecular Nanotechnologies, Istituto Italiano di Tecnologia (IIT), Via Barsanti, I-73010 Arnesano, Italy

[§]Center for Metamaterials and Integrated Plasmonics, Department of Electrical and Computer Engineering, Duke University, Durham, North Carolina 27708, United States

Supporting Information

ABSTRACT: We have combined atomic layer lithography and template stripping to produce a new class of substrates for surface-enhanced infrared absorption (SEIRA) spectroscopy. Our structure consists of a buried and U-shaped metal−insulator−metal waveguide whose folded vertical arms efficiently couple normally incident light. The insulator is formed by atomic layer deposition (ALD) of Al_2O_3 and precisely defines the gap size. The buried nanocavities are protected from contamination by a silicon template until ready for use and exposed by template stripping on demand. The exposed nanocavity generates strong infrared resonances, tightly confines infrared radiation into a gap that is as small as 3 nm ($\lambda/3300$), and creates a dense array of millimeter-long hotspots. After partial removal of the insulators, the gaps are backfilled with benzenethiol molecules, generating distinct Fano resonances due to strong coupling with gap plasmons, and a SEIRA enhancement factor of 10^5 is observed for a 3 nm gap. Because of the wafer-scale manufacturability, single-digit-nanometer control of the gap size via ALD, and long-term storage enabled by template stripping, our buried plasmonic nanocavity substrates will benefit broad applications in sensing and spectroscopy.

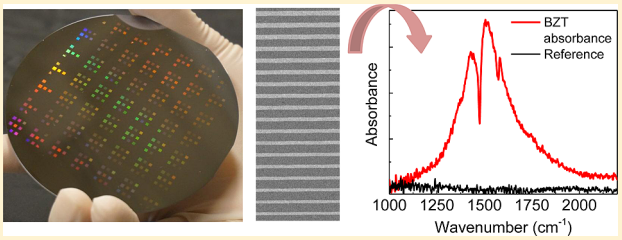

KEYWORDS: *Surface-enhanced infrared absorption (SEIRA), nanogap, template stripping, surface plasmon, gap plasmon, atomic layer deposition, Fano resonance, nanocavity*

Nanometer-scale gaps in noble metals are one of the key building blocks for plasmonic devices.[1−4] Plasmonic nanostructures that are characterized by small gaps can concentrate electromagnetic waves into nanometric volumes, enhancing light−matter interactions in an unprecedented way.[5,6] This unique capability has been utilized for fundamental investigations of nanophotonic phenomena, exposing light-induced electron tunneling[7,8] and nonlocality,[9] as well as for applications in surface-enhanced spectroscopies[1,3,10,11] optical trapping,[12,13] and nonlinear optics.[14] Pointlike nanogaps formed by nearly touching metal nanoparticles have been extensively studied in the context of surface-enhanced Raman spectroscopy (SERS).[7] By the use of flat-sided nanoparticles such as nanocubes or thin-film stacks, it is possible to create extended gaps, forming metal−insulator−metal (MIM) waveguides[2] that can support highly confined electromagnetic modes—gap plasmons[15]—that propagate with no cutoff. As the gap size is reduced to single-digit nanometers and the particle dimensions are kept constant, the resonances of such structures shift toward longer wavelengths, typically out into the near-infrared (near-IR) region. Strong plasmon resonances can in principle also be obtained in the mid-infrared (mid-IR) regime, where lower optical losses than in the visible and near-IR regions make them well-suited for applications such as thermal emission[16] and surface-enhanced infrared absorption (SEIRA).[17,18]

IR absorption spectroscopy is an important analytical technique that complements Raman spectroscopy to acquire molecular vibrational fingerprints in a label-free manner. The small IR absorption cross section of molecules, however, presents a challenge for sensitive detection. In SEIRA, surface-plasmon-enhanced local optical fields boost the IR absorption of molecules adsorbed on metallic surfaces. Various geometries such as metallic islands,[17] nanorods,[19−22] nanoholes,[23] split rings,[24] and nanoshells[7] are utilized to enhance local electromagnetic fields. While isolated metallic structures have shown impressive performance for SEIRA, coupled nanogap structures that take advantage of gap plasmons possess an ideal geometry to maximize field confinement and enhancement, as has been shown for SERS. Plasmonic nanogap structures have been fabricated using electron-beam lithography,[25−27] focused ion beam (FIB),[28,29] electromigration,[3] and nanosphere lithography.[30−32] Reproducible manufacturing of single-digit-nanometer gaps, however, remains a challenge. For broader

Received: August 14, 2014
Revised: November 16, 2014

   dx.doi.org/10.1021/nl503126s | *Nano Lett.* XXXX, XXX, XXX−XXX

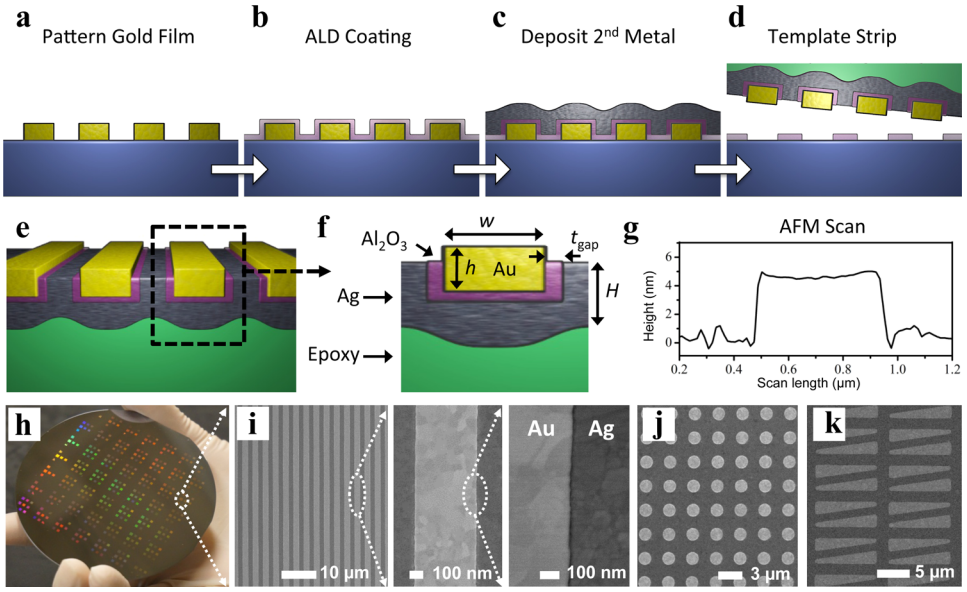

Figure 1. (a–e) Schematic of the device fabrication process. Standard photolithography is used to pattern gold films on a 4 in. silicon wafer. These patterns are conformally encapsulated with a thin alumina spacer using atomic layer deposition (ALD). Next, a silver film is deposited conformally on the pattern, and the whole structure is stripped off the silicon substrate using UV cured epoxy and a glass slide. (f) Cross-sectional schematic of a buried nanocavity. (g) Contact-mode AFM line scan across a 5 nm nanogap cavity showing the height difference between the gold and silver films due to the 5 nm thick Al_2O_3 film. (h) Photograph of a 4 in. wafer containing metal stripes after liftoff. Each square is approximately 1.5 mm × 1.5 mm. (i) SEM image of an array of buried nanogaps on a chip. Further zoomed-in images show a single cavity and a 5 nm nanogap on one side of the cavity. (j, k) SEM images of buried disks and wedges.

dissemination, improved sensitivity, and reproducibility and to relax the requirement of intense sources for SEIRA, it is important to manufacture large-area substrates with dense hotspot arrays.

In addition to direct-write lithography, nanogaps can also be constructed via thin-film deposition.[2,30,33] The key advantage of this approach is that the film thickness can readily be controlled with single-digit-nanometer- or even Ångstrom-scale resolution using atomic layer deposition (ALD). Atomic layer lithography, a new patterning approach based on ALD, can create gaps with sub-nanometer thickness.[34] The present work combines atomic layer lithography with template stripping, which uses silicon templates to produce smooth patterned metals,[35−37] to construct strippable plasmonic nanocavities for SEIRA and achieve strong field enhancements through precise control over the gap size.

As illustrated in Figure 1, our MIM nanocavity is constructed by burying dielectric-coated metal patterns (e.g., stripes, disks) into another metal film. As a result, the nanocavity is folded into a U shape (Figure 1) wherein two vertical arms efficiently couple the incident light. The resultant buried cavity geometry is mechanically robust against wet processing and presents planarized top surfaces that facilitate subsequent integration with other devices or microfluidics. The insulating film in the vertical arms can be removed without compromising the mechanical stability of the cavity and backfilled with analyte molecules for enhanced sensing. Plasmonic hotspots are generated along the entire length of a 1.5 mm long nanocavity, and thus, our structure is robust against local defects or impurities compared with pointlike nanogap structures. Importantly, these cavities are protected by a silicon template and can be exposed via template stripping immediately before use, preventing surface contamination. We show SEIRA spectroscopy results using these structures and distinct Fano resonances due to strong coupling between molecules and gap plasmons.

The process flow for making our nanogap structure is illustrated in Figures 1a–e. First, 80 nm thick gold stripes are patterned on a 4 in. Si wafer using standard photolithography followed by metal evaporation and liftoff. It should be noted that no adhesion layer is used between the gold film and the Si substrate, a necessity for template stripping of the final structure. The gold stripes are then conformally coated with a thin layer of alumina (Al_2O_3) using ALD (Figure 1b). A second layer of metal (150 nm thick silver) is deposited on top of the alumina to form the nanogap between the gold and silver films, with the gap width precisely defined by the thickness of the ALD-grown Al_2O_3 film (Figure 1c). Finally, the nanogap structures are template-stripped and exposed for molecule deposition and spectroscopic measurements. For this template-stripping step, a UV-curable optical adhesive (NOA 61, Norland Products Inc.) is applied to the surface of a silver film (Figure 1d), covered with a glass slide, and cured under a UV lamp and on a hot plate, and the whole structure is stripped off the Si wafer (Figure 1e). A schematic cross section of the buried nanocavity device is illustrated in Figure 1f. We imaged the sample surface of a 5 nm gap pattern with atomic force microscopy (AFM). A line scan (Figure 1g) shows the height difference between the template-stripped gold and silver surfaces due to the thickness of the alumina layer. This height difference arises from the relatively stronger adhesion of alumina to silicon than to silver, as a result of which the alumina film on the flat region is not peeled off during the template-stripping process. Only the alumina film inside the gap is transferred with the sample.

With standard photolithography, any pattern shapes can be produced over a large area (Figure 1h). The scanning electron microscopy (SEM) image in Figure 1i, which was taken after template stripping, shows cavities with a gap size of 5 nm.

dx.doi.org/10.1021/nl503126s | Nano Lett. XXXX, XXX, XXX−XXX

Because the nanogaps are made entirely with wafer-scale batch processes, namely, metal deposition, photolithography, and ALD, there are no limitations on the size and shape of the cavity patterns. It is straightforward to produce a densely packed array of millimeter- or centimeter-long nanocavities over an entire 4 in. Si wafer in any shape, such as disks (Figure 1j) or wedges (Figure 1k). The high packing density combined with millimeter-scale horizontal length (perpendicular to the cavity length direction) facilitates FTIR measurements. A Nicolet Series II Magna-IR System 750 FTIR spectrometer equipped with an IR microscope (15× IR objective lens, NA = 0.58) was used to measure the spectra from the nanogap samples in reflection mode using unpolarized light. The spectrometer and the microscope were purged with dry air. The sample and the light path from the objective lens to the sample were exposed to the atmosphere. An adjustable built-in aperture in the IR microscope was used to define the illumination spot size. We measured absorbance spectra (defined as $\log_{10}(I_o/I)$, where I_o is the reflected signal from a reference bare silver surface and I is the reflected signal from the nanogap cavities) from nanogap cavities with metal stripe widths of 500, 600, 700, 900, 1300, and 1700 nm, each with gap sizes of 3, 5, 7, and 10 nm. The gold film thickness was fixed at 80 nm for all of the samples. Figure 2a shows the spectra measured from 3 nm gap structures with different cavity lengths. Multiple Fabry–Pérot (FP) resonances are observed at wavelengths between 10 and 1.6 μm. Similar FP resonances are also observed in disk-shaped nanocavities (data not shown).

The peaks observed in the spectra shown in Figure 2a correspond to the FP resonances in the buried nanogap cavity.[2,38] While the cavity is folded, the gap plasmon follows the dispersion as if it were propagating in an unfolded nanogap cavity.[39] Although we use unpolarized light to launch gap plasmon modes in our structures, only the TM component (electric field perpendicular to the stripes) couples to the gap plasmon mode in the 2D cavities. Moreover, with normally incident light, only FP modes that are symmetric with respect to the magnetic field can be excited. In our experiments, antisymmetric modes were also observed as small peaks between the much stronger resonance peaks associated with the symmetric modes because the incident light was not perfectly collimated (NA = 0.58). Simulation results show that the leftmost peak of each spectrum in Figure 2a is the first symmetric FP mode.

As with other MIM cavity structures, spectral scaling can be simply achieved by tuning the cavity length or the gap thickness. Increasing the cavity length shifts the FP modes toward longer wavelengths. With micron-scale cavity lengths fabricated using photolithography, the cavity resonance can be tuned from the mid- to near-IR. Submicron-scale cavities fabricated via electron-beam lithography can possess resonances in the visible regime, which will be the focus of future work. Many high-order FP modes are observed from longer cavities. Figure 2b shows a reflection spectrum obtained from a 5 nm gap cavity plotted as a function of wavelength, which shows a series of sharp resonances peaks. A Q factor (defined as $\lambda_{resonance}/\Delta\lambda$) of 34 was measured at a resonance wavelength of 1.8 μm. For a decreasing gap thickness, these resonances shift toward longer wavelengths because of the gap plasmon dispersion.[40] That is, as the gap shrinks, the effective refractive index of the tightly confined plasmonic mode grows, increasing the effective cavity length and thus the resonant wavelength.

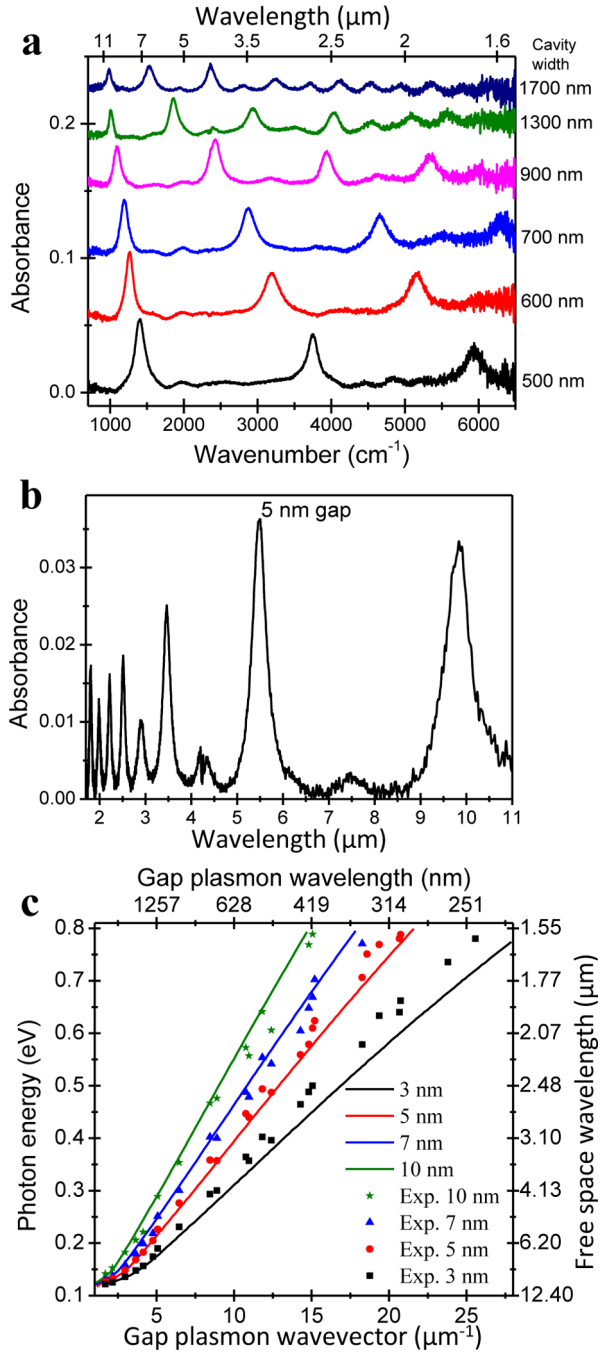

Figure 2. Mid-IR spectra and dispersion of gap plasmons. (a) FTIR spectra from 3 nm gap cavities in a 2D stripe pattern with different metal stripe widths. Spectra are offset in the y direction for clarity. See the Supporting Information for measured spectra from 5, 7, and 10 nm nanogap cavities. (b) FTIR spectrum measured from a 5 nm gap cavity in a 2D stripe pattern with a cavity width of 1700 nm, plotted vs wavelength. (c) Nanogap dispersion from experimental and simulation data for 3, 5, 7, and 10 nm gaps. The solid lines were plotted using the theoretical dispersion curve for gap plasmons[2] (see the Supporting Information) for different cavity lengths and gap sizes.

Using the peak resonance wavelength, we can deduce the dispersion characteristics of the gap plasmon in buried nanocavities, as shown in Figure 2c for gap sizes of 3, 5, 7, and 10 nm. The results obtained using an analytical dispersion equation for 2D gap plasmons[2,41] are shown as the solid lines in Figure 2c. For the wider gaps (7 and 10 nm in width), the

dx.doi.org/10.1021/nl503126s | Nano Lett. XXXX, XXX, XXX–XXX

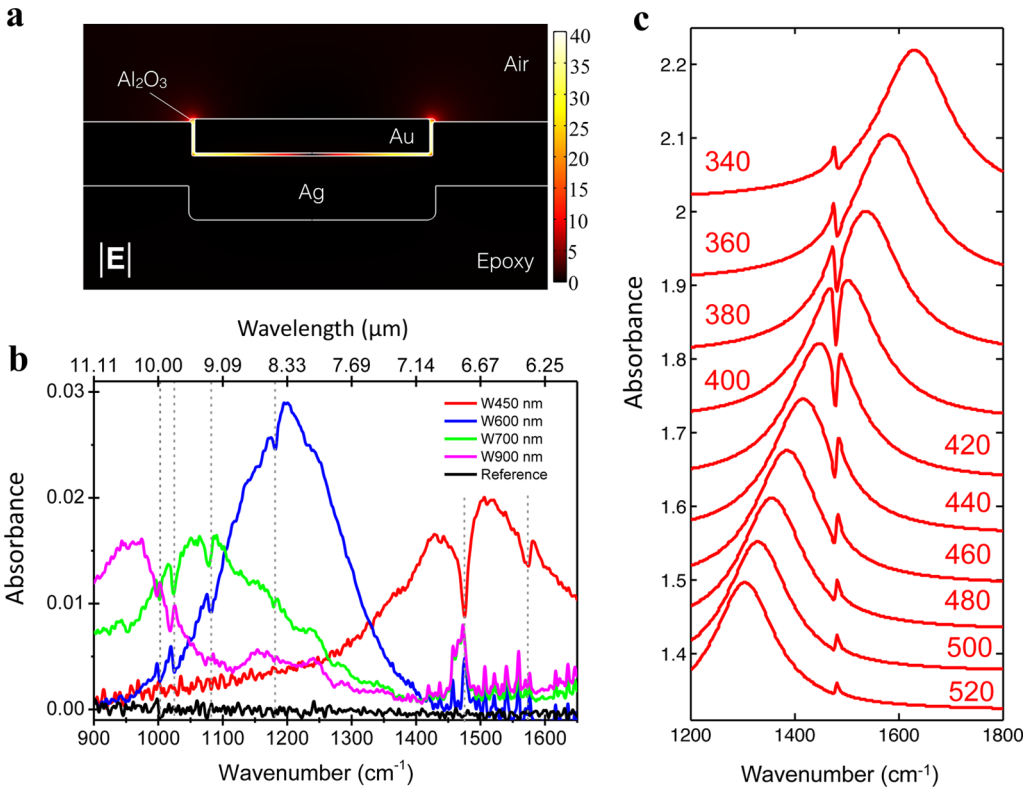

Figure 3. (a) Field distribution in the buried nanogap. The field strength is highest at the nanogap outlets. (b) Sensing of benzenethiol using a buried 3 nm gap with various stripe widths. The black curve is the absorption of a BZT monolayer coated on a template-stripped (TS) silver film without any pattern. It should be noted that the absorption from the BZT monolayer is below the noise level. The vertical gray dashed lines in the figure indicate the absorption bands of BZT. (c) Simulated Fano coupling between BZT absorption and gap plasmon resonance in nanogap devices with various metal stripe widths ranging from 340 to 520 nm.

theoretical and experimental data are in good agreement. For the 3 and 5 nm gaps, the experimental data deviate toward shorter wavelengths compared with the theoretical predictions, likely because of the roughness of the metal surface in the nanogap. For the 3 nm gap, we find an effective refractive index of 6.5 for the gap plasmon mode. The resonance peak measured for this sample at a wavelength of 10.16 μm indicates that free-space radiation can be squeezed into a cavity as narrow as 3 nm (λ/3300), demonstrating the strong optical confinement enabled by the MIM geometry.

It is interesting to note that the spectra shown in Figure 2a exhibit very distinct peak resonances, which is indicative of good coupling between the gap plasmon and far-field modes. This coupling is quite remarkable for the structure consisting of bare metal for more than 99.5% of its topographically flat surface. The strong coupling can be understood intuitively by replacing the fields radiated by the slits (formed by the vertical arms of the cavity) with effective magnetic currents that re-emit a wave whose field has the opposite phase to the scattered wave reflecting off the metal region. The resultant destructive interference reduces the total reflected field, greatly enhancing the energy absorbed from the incident wave.[40,42]

After mapping the resonances of the nanocavity structures, we coated the exposed cavities with a monolayer of benzenethiol (BZT) molecules to perform nanogap-enhanced IR absorption spectroscopy. Finite-element method (FEM) calculations using COMSOL, a commercially available finite-element-based solver, predict that the strongest electric field of the first FP mode exists at the end facets of the nanogap cavity, with a simulated field intensity ($|E|^2$) enhancement of about 1600 (Figure 3a). To utilize the maximum near-field strength inside the gap, molecules should be placed inside the gap region, which is initially filled with the Al_2O_3 film. To accomplish this, buffered oxide etch (BOE) was used to partially remove Al_2O_3 inside the nanogap (see the Supporting Information for details). After cleaning with DI water and drying with nitrogen, the sample was soaked in a 2 mM benzenethiol solution in ethanol for 24 h to coat the exposed gold and silver surfaces with a monolayer of BZT.[43] Excess BZT was removed by cleaning with ethanol. The spectra from BZT-coated samples were then measured by FTIR (Figure 3b). Six absorption peaks in the mid-IR for BZT (1000, 1022, 1073, 1181, 1473, and 1575 cm^{-1}) are in the resonant range of our nanogap structures, which runs from 10 to 6 μm. The first-order resonance of our device can be tuned from 6 to 11.5 μm (with a measured spectral line width of less than 1 μm) by changing the width of the metal stripes from 450 to 900 nm. Enhancement factors (EFs) of up to 10^5, which are comparable to EFs measured from other high-performance SEIRA substrates, were calculated using experimental data (for details, see the Supporting Information). These EFs are also in the range predicted by our numerical simulations if the normalization of the field enhancement is calculated with respect to the local fields at a silver surface (usually <10%).

The measured spectra show an asymmetric Fano-shape resonance[19,21,44,45] for each absorption band, a behavior confirmed by numerical calculations. The BZT monolayer can be modeled as a thin layer whose dielectric function is obtained as a sum of Lorentz oscillators that match the absorption resonances of the BZT molecule. For the sake of

dx.doi.org/10.1021/nl503126s | Nano Lett. XXXX, XXX, XXX−XXX

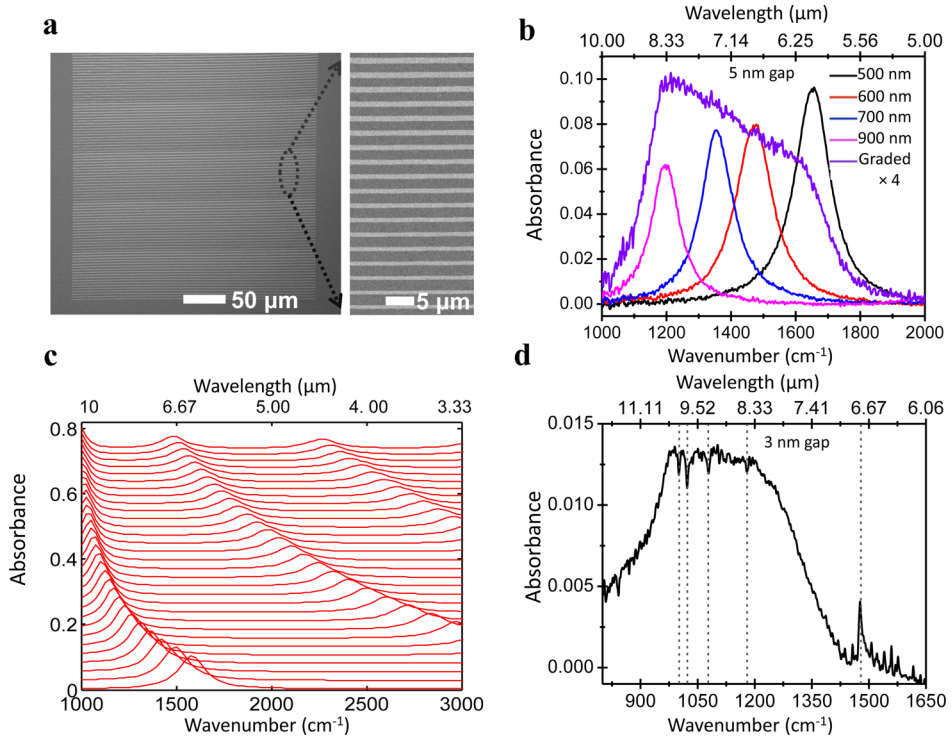

Figure 4. Tunable broadband resonators. (a) SEM images of a nanocavity array with varying metal stripe widths. The zoomed-in image shows a section of the device wherein the width of the metal stripes (brighter regions) increases from 500 nm (bottom) to 1010 nm (top). (b) FTIR spectrum (purple line) from nanogap cavities with metal stripe widths ranging from 500 to 1010 nm in 30 nm steps on a single device (multiplied by 4 for comparison). Spectra from 5 nm gaps with single widths (500, 600, 700, and 900 nm) on one device (black, red, blue, and pink lines, respectively) are also plotted. The spectra were measured from an area of approximately 130 μm × 130 μm. (c) Simulation of a 5 nm nanocavity with various metal stripe widths. (d) Sensing of benzenethiol using a graded nanogap structure with a gap size of 3 nm. Gray dashed lines indicate BZT absorption peaks.

clarity, however, we considered just one oscillator corresponding to the main resonance at 1473 cm^{-1}. As for the actual experimental sample, we intercalated BZT roughly 3 nm into the gap (controlled by the BOE processing time) to increase the coupling with the gap plasmon mode of the structure. A set of reflection spectra calculated for different stripe widths are shown in Figure 3c. As the resonance of the system is shifted across the BZT absorption resonance, very distinct Fano-shape features appear in the reflection spectra. These resonances are qualitatively identical to those shown in Figure 3b depending on the relative position of the BZT absorption peak with respect to the gap plasmon resonance.

By combination of nanogaps with different cavity lengths, it is possible to create a broadband plasmonic resonator that covers a wide spectral region of the mid-IR fingerprint region. Similar ideas have been used by others to obtain broadband resonances from engineered optical antennas.[46,47] As shown in Figure 4a, we made an array of metal stripes with widths ranging from 500 to 1010 nm in 30 nm steps. The spectrum from this laterally graded cavity resonator is shown in Figure 4b. Resonances from nanogap cavities consisting of uniform metal stripe widths of 500, 600, 700, 900, and 1300 nm are also plotted in the same figure. The device with laterally graded nanocavities possesses a resonance 5−6 times wider than those of the single-cavity-length resonators. We confirmed this observation by simulating a nanogap cavity with metal stripe widths from 500 to 1000 nm with 50 nm steps, as shown in Figure 4c. We found that the first resonance mode from each device spans a wavelength range from 11 to 6 μm, covering the typical mid-IR fingerprinting region for molecules. A laterally graded nanogap structure with a 3 nm gap size was used for BZT sensing to demonstrate the functionality of the broadband resonator (Figure 4d).

In summary, we have combined atomic layer lithography and template stripping to fabricate buried plasmonic nanocavity arrays at the wafer scale with a minimum gap size of 3 nm. These new class of substrates for SEIRA can generate intense gap plasmons that boost coupling of IR radiation with molecules situated in the gaps. High SEIRA enhancements of up to 5 orders of magnitude have been observed. As the hotspots of each nanocavity uniformly extend along millimeter-long lines, our substrates are robust against localized defects or contaminants, which will enable more reproducible SEIRA spectroscopy and also the combination of SERS and SEIRA on the same substrate.[48] As with other template-stripped metallic nanostructures,[49] the surfaces and high-field areas of these strippable nanocavities are initially protected by a silicon template, which provides a robust protection mechanism against contamination or degradation, and thus, each chip can be stored for an extended time and template-stripped on-demand. Smaller gap dimensions (down to 1 nm) are achievable using atomic layer lithography,[34] even though they were not needed for the molecular sensing experiments performed here. Because the Au and Ag films are electrically isolated by an insulating layer, applying a bias across the gap can turn these structures into vertically oriented tunnel junctions. Such structures can be used to study electron tunneling[50] and nonlocal electrodynamics[9] as well as for photodetection.[51]

dx.doi.org/10.1021/nl503126s | Nano Lett. XXXX, XXX, XXX−XXX

■ ASSOCIATED CONTENT

Supporting Information

Detailed fabrication methods, FTIR instrument and measurement, surface functionalization, and calculation of SEIRA enhancement factors. This material is available free of charge via the Internet at http://pubs.acs.org.

■ AUTHOR INFORMATION

Corresponding Author

*E-mail: sang@umn.edu.

Notes

The authors declare no competing financial interest.

■ ACKNOWLEDGMENTS

This research was supported by the U.S. Department of Defense (DARPA Young Faculty Award N66001-11-1-4152; X.C. and S.-H.O.), the Office of Naval Research Young Investigator Program (S.-H.O.), the Air Force Office of Scientific Research (AFOSR, Grant FA9550-12-1-0491; C.C. and D.R.S.), and the Army Research Office through a Multidisciplinary University Research Initiative (Grant W911NF-09-1-0539; C.C. and D.R.S.). The team also utilized resources at the University of Minnesota, including the Nanofabrication Center, which receives partial support from NSF through the National Nanotechnology Infrastructure Network, and the Characterization Facility, which has received capital equipment from NSF MRSEC. X.C. acknowledges support from the 3M Science and Technology Fellowship and the University of Minnesota Doctoral Dissertation Fellowship. The authors thank Jonah Shaver for helpful comments.

■ REFERENCES

(1) Xu, H.; Bjerneld, E.; Käll, M.; Borjesson, L. *Phys. Rev. Lett.* **1999**, *83*, 4357−4360.
(2) Miyazaki, H. T.; Kurokawa, Y. *Phys. Rev. Lett.* **2006**, *96*, No. 097401.
(3) Ward, D. R.; Grady, N. K.; Levin, C. S.; Halas, N. J.; Wu, Y.; Nordlander, P.; Natelson, D. *Nano Lett.* **2007**, *7*, 1396−1400.
(4) Halas, N. J. *Nano Lett.* **2010**, *10*, 3816−3822.
(5) García-Vidal, F. J.; Martin-Moreno, L.; Ebbesen, T. W.; Kuipers, L. *Rev. Mod. Phys.* **2010**, *82*, 729−787.
(6) Gramotnev, D. K.; Bozhevolnyi, S. I. *Nat. Photonics* **2010**, *4*, 83−91.
(7) Halas, N. J.; Lal, S.; Chang, W.-S.; Link, S.; Nordlander, P. *Chem. Rev.* **2011**, *111*, 3913−3961.
(8) Esteban, R.; Borisov, A. G.; Nordlander, P.; Aizpurua, J. *Nat. Commun.* **2012**, *3*, No. 825.
(9) Ciracì, C.; Hill, R. T.; Mock, J. J.; Urzhumov, Y.; Fernandez-Dominguez, A. I.; Maier, S. A.; Pendry, J. B.; Chilkoti, A.; Smith, D. R. *Science* **2012**, *337*, 1072−1074.
(10) Moskovits, M. *Rev. Mod. Phys.* **1985**, *57*, 783−826.
(11) Haynes, C. L.; McFarland, A.; Van Duyne, R. P. *Anal. Chem.* **2005**, *77*, 338A−346A.
(12) Xu, H.; Käll, M. *Phys. Rev. Lett.* **2002**, *89*, No. 246802.
(13) Pang, Y.; Gordon, R. *Nano Lett.* **2012**, *12*, 402−406.
(14) Danckwerts, M.; Novotny, L. *Phys. Rev. Lett.* **2007**, *98*, No. 026104.
(15) Moreau, A.; Ciracì, C.; Smith, D. R. *Phys. Rev. B* **2013**, *87*, No. 045401.
(16) Ikeda, K.; Miyazaki, H. T.; Kasaya, T.; Yamamoto, K.; Inoue, Y.; Fujimura, K.; Kanakugi, T.; Okada, M.; Hatade, K.; Kitagawa, S. *Appl. Phys. Lett.* **2008**, *92*, No. 021117.
(17) Osawa, M. *Top. Appl. Phys.* **2001**, *81*, 163−187.
(18) Lal, S.; Grady, N. K.; Kundu, J.; Levin, C. S.; Lassiter, J. B.; Halas, N. J. *Chem. Soc. Rev.* **2008**, *37*, 898−911.
(19) Neubrech, F.; Pucci, A.; Cornelius, T.; Karim, S.; García-Etxarri, A.; Aizpurua, J. *Phys. Rev. Lett.* **2008**, *101*, No. 157403.
(20) Aksu, S.; Yanik, A. A.; Adato, R.; Artar, A.; Huang, M.; Altug, H. *Nano Lett.* **2010**, *10*, 2511−2518.
(21) Giannini, V.; Francescato, Y.; Amrania, H.; Phillips, C. C.; Maier, S. A. *Nano Lett.* **2011**, *11*, 2835−2840.
(22) Brown, L. V.; Zhao, K.; King, N.; Sobhani, H.; Nordlander, P.; Halas, N. J. *J. Am. Chem. Soc.* **2013**, *135*, 3688−3695.
(23) Coe, J. V.; Heer, J. M.; Teeters-Kennedy, S.; Tian, H.; Rodriguez, K. R. *Annu. Rev. Phys. Chem.* **2008**, *59*, 179−202.
(24) Cubukcu, E.; Zhang, S.; Park, Y.-S.; Bartal, G.; Zhang, X. *Appl. Phys. Lett.* **2009**, *95*, No. 043113.
(25) Schuck, P. J.; Fromm, D. P.; Sundaramurthy, A.; Kino, G. S.; Moerner, W. E. *Phys. Rev. Lett.* **2005**, *94*, No. 017402.
(26) Koh, A. L.; Fernandez-Dominguez, A. I.; McComb, D. W.; Maier, S. A.; Yang, J. K. W. *Nano Lett.* **2011**, *11*, 1323−1330.
(27) Huck, C.; Neubrech, F.; Vogt, J.; Toma, A.; Gerbert, D.; Katzmann, J.; Härtling, T.; Pucci, A. *ACS Nano* **2014**, *8*, 4908−4914.
(28) Choo, H.; Kim, M.-K.; Staffaroni, M.; Seok, T. J.; Bokor, J.; Cabrini, S.; Schuck, P. J.; Wu, M. C.; Yablonovitch, E. *Nat. Photonics* **2012**, *6*, 838−844.
(29) Melli, M.; Polyakov, A.; Gargas, D.; Huynh, C.; Scipioni, L.; Bao, W.; Ogletree, D. F.; Schuck, P. J.; Cabrini, S.; Weber-Bargioni, A. *Nano Lett.* **2013**, *13*, 2687−2691.
(30) Wang, H.; Levin, C. S.; Halas, N. J. *J. Am. Chem. Soc.* **2005**, *127*, 14992−14993.
(31) Im, H.; Bantz, K. C.; Lee, S. H.; Johnson, T. W.; Haynes, C. L.; Oh, S.-H. *Adv. Mater.* **2013**, *25*, 2678−2685.
(32) Hoffmann, J. M.; Janssen, H.; Chigrin, D. N.; Taubner, T. *Opt. Express* **2014**, *22*, 14425−14432.
(33) Im, H.; Bantz, K. C.; Lindquist, N. C.; Haynes, C. L.; Oh, S.-H. *Nano Lett.* **2010**, *10*, 2231−2236.
(34) Chen, X.; Park, H.-R.; Pelton, M.; Piao, X.; Lindquist, N. C.; Im, H.; Kim, Y. J.; Ahn, J. S.; Ahn, K. J.; Park, N.; Kim, D.-S.; Oh, S.-H. *Nat. Commun.* **2013**, *4*, No. 2361.
(35) Nagpal, P.; Lindquist, N. C.; Oh, S.-H.; Norris, D. J. *Science* **2009**, *325*, 594−597.
(36) Lindquist, N. C.; Johnson, T. W.; Norris, D. J.; Oh, S.-H. *Nano Lett.* **2011**, *11*, 3526−3530.
(37) Lindquist, N. C.; Nagpal, P.; McPeak, K. M.; Norris, D. J.; Oh, S.-H. *Rep. Prog. Phys.* **2012**, *75*, No. 036501.
(38) Alaee, R.; Menzel, C.; Huebner, U.; Pshenay-Severin, E.; Bin Hasan, S.; Pertsch, T.; Rockstuhl, C.; Lederer, F. *Nano Lett.* **2013**, *13*, 3482−3486.
(39) Petschulat, J.; Helgert, C.; Steinert, M.; Bergner, N.; Rockstuhl, C.; Lederer, F.; Pertsch, T.; Tünnermann, A.; Kley, E.-B. *Opt. Lett.* **2010**, *35*, 2693−2695.
(40) Moreau, A.; Ciracì, C.; Mock, J. J.; Hill, R. T.; Wang, Q.; Wiley, B. J.; Chilkoti, A.; Smith, D. R. *Nature* **2012**, *492*, 86−89.
(41) Kurokawa, Y.; Miyazaki, H. T. *Phys. Rev. B* **2007**, *75*, No. 035411.
(42) Ciracì, C.; Lassiter, J. B.; Moreau, A.; Smith, D. R. *J. Appl. Phys.* **2013**, *114*, No. 163108.
(43) Haynes, C. L.; Van Duyne, R. P. *J. Phys. Chem. B* **2003**, *107*, 7426−7433.
(44) Luk'yanchuk, B.; Zheludev, N. I.; Maier, S. A.; Halas, N. J.; Nordlander, P.; Giessen, H.; Chong, C. T. *Nat. Mater.* **2010**, *9*, 707−715.
(45) Wu, C.; Khanikaev, A. B.; Adato, R.; Arju, N.; Yanik, A. A.; Altug, H.; Shvets, G. *Nat. Mater.* **2012**, *11*, 69−75.
(46) Aouani, H.; Šípová, H.; Rahmani, M.; Navarro-Cia, M.; Hegnerová, K.; Homola, J.; Hong, M.; Maier, S. A. *ACS Nano* **2013**, *7*, 669−675.
(47) Aydin, K.; Ferry, V. E.; Briggs, R. M.; Atwater, H. A. *Nat. Commun.* **2011**, *2*, No. 517.
(48) Le, F.; Brandl, D. W.; Urzhumov, Y. A.; Wang, H.; Kundu, J.; Halas, N. J.; Aizpurua, J.; Nordlander, P. *ACS Nano* **2008**, *2*, 707−718.
(49) Johnson, T. W.; Lapin, Z. J.; Beams, R.; Lindquist, N. C.; Rodrigo, S. G.; Novotny, L.; Oh, S.-H. *ACS Nano* **2012**, *6*, 9168−9174.

(50) Bharadwaj, P.; Bouhelier, A.; Novotny, L. *Phys. Rev. Lett.* **2011**, *106*, No. 226802.
(51) Knight, M. W.; Sobhani, H.; Nordlander, P.; Halas, N. J. *Science* **2011**, *332*, 702−704.